Check for updates

Removal of tetracycline antibiotics from agricultural wastewater efficiently using natural attapulgite functionalized MIL-53(Fe): adsorption mechanism and thermodynamic study†

Jiaolan Liu,[a] Xiaoyan Wang,[b] Yuzhu Yang,[a] Wei Liu*[b] and Wei Sheng Liu ✱*[a]

An excessive utilization of tetracycline antibiotics (TCs) in aquaculture and livestock farming significantly threatens human health and the vitality of aquatic environments. In this work, we used a one-pot hydrothermal approach with APT@MIL53-*X* hybrid material to achieve the selective removal of TC and OTC from agricultural wastewater. APT@MIL53-*X* showed significant chemical stability in the 3–10 pH range. Analysis of the adsorption results using adsorption kinetics, adsorption isotherm studies and adsorption thermodynamics indicated the presence of a monolayer physicochemical adsorption process with a maximum equilibrium adsorption of 600.43 mg g^{-1} for TC (removal efficiency of 93.5%) and 537.71 mg g^{-1} for OTC (removal efficiency of 91.4%). The elimination of TCs was not significantly impacted by the common buffer system of solution or the presence of water. Furthermore, a number of characterization techniques, including FT-IR and XPS, suggested that electrostatic interactions, $\pi-\pi$ stacking, and hydrogen were potential adsorption processes. APT@MIL53-*X* showed stable recycling performance, maintaining a stable adsorption amount and chemical stability after six adsorption–desorption cycles of use, which proved that APT@MIL53-*X* has application possibilities for the agricultural wastewater treatment process. This study illustrates that APT@MIL53(Fe)-*X* hybrid material offers a novel method for the selective and effective elimination of agricultural wastewater.

1. Introduction

In the past few decades, an ongoing rise in the global population and the concomitant rapid advancement of industrial, urban, and agrochemical practices,[1] including pollution resulting from the extensive use of antibiotics and pharmaceuticals,[2] have presented unparalleled challenges to human health and ecological water environments.[2] The issue arises from the incomplete consumption of antibiotics, attributable to their intricate structure and challenging degradation in aquatic organisms.[3] Consequently, up to 75% of the antibiotics utilized enter the ecological hydrological cycle as effluents, leading to the emergence of resistant microorganisms and genes,[4] thereby jeopardizing human health and ecological water security. Tetracycline antibiotics (TCs) are regarded as among the most economical antibiotics, with tetracycline (TC) and

oxytetracycline (OTC) being ideally utilized,[5] and their indiscriminate application has resulted in the detection of tetracycline in some drinking water sources, raising concerns regarding human and animal health as well as environmental harm. TC/OTC is not fully eliminated by conventional treatment methods due to its considerable persistence in agricultural aquaculture wastewater, attributed to its notable biotoxicity,[6] high hydrophilicity, and extended half-life (34–329 h),[7] along with other tricky characteristics. Hence, it is imperative to identify water treatment technologies that mitigate antibiotic residues in agricultural water ecosystems and prevent the ecological harm associated with the rise of resistant genes.

Recently, traditional agricultural wastewater treatment technologies (*e.g.* activated carbon, membrane filtration, and ion exchange) have proven notable weaknesses regarding inefficiency and low recycling rates for the removal of TC/OTC.[8] To overcome the constraints of these shortcomings, researchers have devised a range of advanced techniques for the remediation of antibiotics in agricultural wastewater,[9,10] including adsorption technology,[11,12] ultraviolet treatment,[13] and photocatalytic degradation technology.[14–16] The adsorption technique stands out as competitive in practical applications due to its distinctive advantages, including ease of operation, low cost and high removal efficiency.[17] The urgent need for the

*a*Key Laboratory of Nonferrous Metal Chemistry and Resources Utilization of Gansu Province, State Key Laboratory of Applied Organic Chemistry, College of Chemistry and Chemical Engineering, Lanzhou University, Lanzhou 730000, China

*b*Frontiers Science Center for Rare Isotope, Institute of National Nuclear Industry, School of Nuclear Science and Technology, Lanzhou University, Lanzhou, 730000, China

† Electronic supplementary information (ESI) available. See DOI: https://doi.org/10.1039/d5ra00113g

development of environmentally friendly, cost-effective, and practical adsorption materials to mitigate the excessive use of antibiotics in aquatic environments has become increasingly pressing.

Fortunately, metal–organic frameworks (MOFs) are advanced porous materials that have emerged following traditional materials,[18] exhibiting characteristics such as tenability and ease of modification while also enhancing the removal of TC/OTC compared to conventional wastewater treatment methods.[19] MIL-53(Fe), characterized by its superior adsorption capabilities and prospective unsaturated metal active sites, along with low toxicity,[11,20,21] presents a promising application for the adsorptive removal of TC/OTC from agricultural wastewater. However, to prevail over the lack of water stability of MIL-53(Fe), its modification, tailoring, and hybrids are essential to compensate for its limited surface active sites and poor water stability. Previous investigations by the research team demonstrated that environmentally friendly attapulgite (APT) not only can eliminate TC/OTC from wastewater through adsorption,[22,23] but also significantly enhances the water stability of MOF materials,[24–26] indicating substantial potential for investment in MIL-53(Fe) functional hybrid material.

In this work, we have prepared APT@MIL-53(Fe)-X (X is a different percentage example) hybrid material by hybridizing natural APT with MIL-53(Fe) via hydrothermal reaction for efficient TC/OTC removal from agricultural wastewater, that much higher than marketed materials. The adsorption selectivity of TC/OTC was investigated based on the hybrid levels, APT@MIL53(Fe)-70 with 70% APT hybridizing exhibited selective adsorption of TC, while APT@MIL53(Fe)-50 with 50% hybridizing selectively adsorbed OTC. The structural and physicochemical characteristics of APT@MIL-53(Fe)-X were examined through systematic characterization. Selective adsorption for the removal of TC/OTC under single factors effects experiments and simulated agricultural wastewater circumstances were also investigated. Kinetic models, isotherm studies, and adsorption thermodynamics were used to investigate the adsorption process of TC/OTC adsorption. Ultimately, the adsorption mechanisms of APT@MIL-53(Fe)-70 and APT@MIL53(Fe)-50 on TC/OTC were unraveled by comparing the characterization of the hybrid material before and after adsorption. This study addressed the issue of inadequate water stability of MIL-53(Fe) in agricultural wastewater management and introduced a cost-effective, eco-friendly, and efficient novel adsorbent material for the removal of TC/OTC.

2. Experimental section

2.1 Preparation of APT@MIL-53(Fe)-X hybrid material

Preparation of attapulgite (APT) by purification of previous methods.[27] Based on the methodology used to prepare MIL-53(Fe) in the previous,[11,21] 0.709 g of APT, 0.665 g of FeCl$_3$·6H$_2$O, also 0.428 g of terephthalic acid (H$_2$BDC) were obtained. In addition, 0.501 g of APT, 0.655 g of FeCl$_3$·6H$_2$O, and 0.435 g of H$_2$BDC, respectively, were taken, and 15 mL of N,N-dimethylformamide (DMF) was added. After mixing and continuing to ultrasonic for 0.5 h to form a homogeneous solution, the

mixture was transferred into a reactor liner and hydrothermally reacted for 10 h at 423 K. The orange-colored powdered material was obtained by centrifugal washing with ethanol and water until the solution was cleared (ESI: Fig. S1†), followed by activation in an oven at 423 K for 12 h.

2.2 Batch adsorption experiments

As opposed to hybrid materials with varying hybridizing levels, APT hybrid with 70% and 50% of hybrid material had the best adsorption effect for TC/OTC (ESI: Text S3, Table S1 and Fig. S2†), respectively. Therefore, the performance of APT@MIL53(Fe)-70 adsorption for TC removal and APT@MIL53(Fe)-50 adsorption for OTC removal was the main focus. In this case, the removal rate (removal efficiency/%) and adsorption amount (q_t) (mg g^{-1}) of the adsorption performance were measured and computed as follows:[28]

$$R_e(\%) = \frac{(C_0 - C_t)}{C_0}$$

$$q_t = \frac{(C_0 - C_t) \times V}{m}$$

where C_t (mg L^{-1}) is the sampling concentration at time t (min) and C_0 (mg L^{-1}) is the pollutant of antibiotic initial concentration, respectively. V (L) is the volume of the antibiotic pollutant that needs to be treated, and m (g) is the mass of the hybridized adsorbent.

In order to study the effect of adsorption on antibiotic pollutants in agricultural wastewater, a TC/OTC solution with a concentration of 100 mg g^{-1} and a volume of 10 mL was finally selected for the adsorption experiments in 20 mL bottles after selection of conditions (ESI: Text S3†). Under different temperature gradients (288 K, 298 K, 308 K, and 318 K), samples were collected using a syringe at regular intervals of 10, 20, 30, 40, 50, 60, and 120 min in a dark environment. Simultaneously, adsorption isotherms were established at the same temperature gradient. Solutions of TC and OTC with concentrations ranging from 10 mg L^{-1} to 160 mg L^{-1} were prepared, and samples were collected for analysis under dark conditions for 300 min.

3. Results and discussion

Studying the charge of antibiotic distribution before testing is crucial since it will enable more accurate targeted adsorption investigations. Some functional groups in the TC structure are ionized and exist in various forms (Fig. 1a and b). The ionization equilibrium constants of TC are 3.30, 7.69, and 9.69, resulting in four ionized forms: TCH$_3^+$, TCH$_2^\pm$, TCH$_2^-$, and TC^{2-}.[2,22] The susceptible ionization structure of OTC is depicted in Fig. 1d and is presented in the form illustrated in Fig. 1e. The equilibrium constants are 3.57, 7.49, and 9.88, at which point it occurs in four forms: H$_3$OTC$^+$, H$_2$OTC$^\pm$, HOTC$^-$, OTC^{2-}.[2,23] As the pH increases from 3 to 10, the surface charge of the material transitions from positive to negative, with the isoelectric point (pH$_{pzc}$) representing the pH at which the charge is neutral.[29]
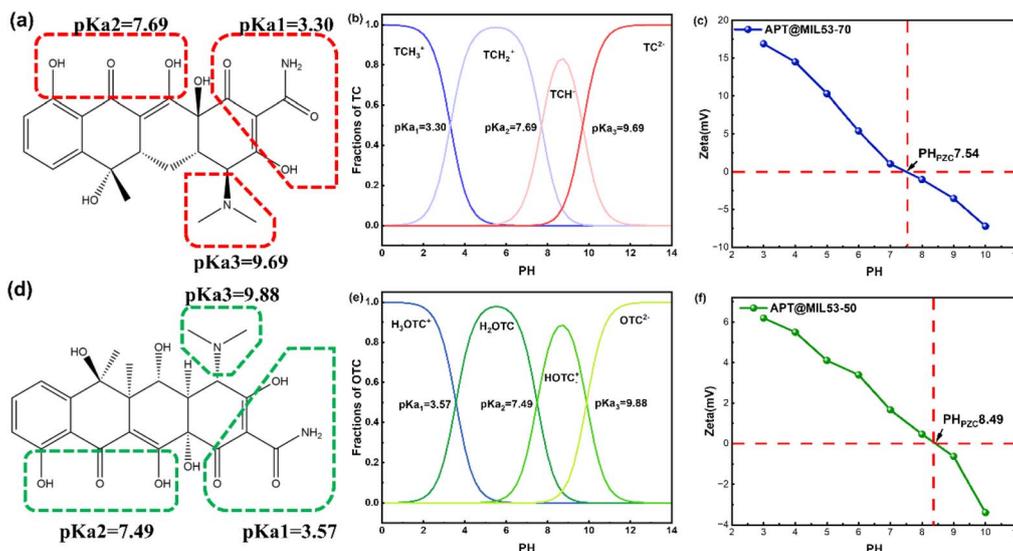
Fig. 1 Structure and partial ionization (a) TC, (d) OTC; ionization equilibrium and form of existence distribution (b) TC, (e) OTC; zeta test of (c) APT@MIL53(Fe)-70, (f) APT@MIL53(Fe)-50.

pH$_{pzc}$ for APT@MIL53(Fe)-70 and APT @MIL53-50(Fe) were 7.54 and 8.49 respectively (Fig. 1c and f).

Beginning with X-ray powder diffraction (PXRD) of APT, MIL-53(Fe), and hybrid material with varying amounts of APT during the preparation process, the produced materials were thoroughly characterized (Fig. 2a). The distinctive diffraction peaks of APT exhibit five principal peaks at 8.8°, 13.9°, 16.7°, 20.0°, and 27.69°, corresponding to the (1 1 0), (2 0 0), (1 3 0), (0 4 0), and (4 0 0) crystallographic planes.[27,30] These characteristic diffraction peaks align consistently with the standard APT

signal peaks (PDF #31-0783), indicating that the APT structure is well crystallized. MIL-53(Fe) has three prominent peaks at 9.2°, 18.6°, and 28.1°, corresponding to the (1 0 1), (0 0 2), and (3 0 2) crystal planes, respectively.[31] The clarity and sharpness of these peaks indicate a homogeneous crystalline structure with few impurities. Both APT@MIL53(Fe)-50 and APT@MIL53(Fe)-70 displayed distinctive peaks akin to those of APT and MIL-53(Fe), signifying the successful synthesis of the hybrid material.[32] As the extent of APT hybridization rises, the peak at the 8.8° point of the hybrid material becomes more pronounced. In
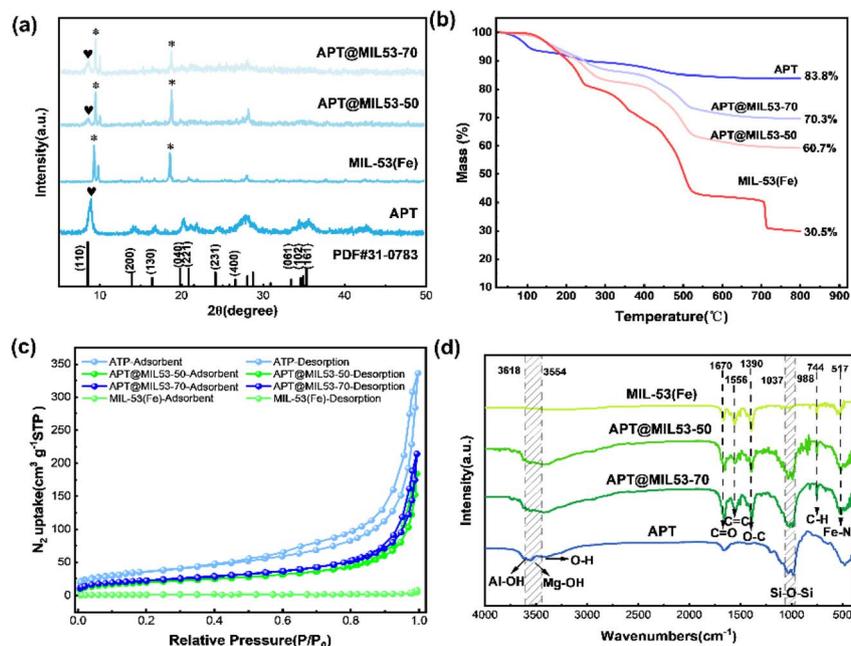

Fig. 2 PXRD patterns of selected samples (a); TGA weight loss analysis (b); N$_2$ adsorption–desorption plots of selected samples (c) FT-IR spectrum of selected samples (d).

Table 1 N₂ adsorption–desorption results at temperature 78 K conditions

Sample	S_{BET} (m² g⁻¹)	V_{total} (cm³ g⁻¹)	Average pore width (nm)
ATP	125.59	0.53	19.00
APT@MIL53(Fe)-70	81.88	0.34	24.61
APT@MIL53(Fe)-70-TC	49.44	0.18	19.30
APT@MIL53(Fe)-50	70.56	0.29	27.27
APT@MIL53(Fe)-50-OTC	39.21	0.17	19.04
MIL-53(Fe)	25.93	0.11	40.61

conclusion, the hybrid materials APT@MIL53-50(Fe) and APT@MIL53(Fe)-70, which are distinct from one another, were effectively synthesized. For evaluation of the thermal stability of the materials, we characterized APT, MIL-53(Fe), and hybrid materials with varying APT hybridizing through thermogravimetric analysis (TGA). The APT depicted in Fig. 2b demonstrates that with rising temperature, surface-bound water, zeolite water, and ligand water molecules are sequentially removed within the structure. APT has significant thermal stability. MIL-53(Fe) exhibits a sequential removal of residual solvent from its surface, a loss of the distributor within the crystal structure,[33] a significant reduction in the weight of the majority of the ligand and its functional groups, and ultimately, the collapse of the organic framework of MIL-53(Fe), resulting in an overall weight loss of 60.5%.[14] Following APT mixing, the weighted platforms of the mixed materials APT@MIL53(Fe)-70 and APT@MIL53(Fe)-50 exhibited similarity, however, the weight loss varied. After weighting of APT comparable to MIL-53(Fe), the material experienced a weight reduction of 29.7%, while the weight of matter constituted 39.3%. There is a notable decrease in weight loss and a considerable enhancement in the thermal stability of the hybrid material with increased APT hybrids compared to MIL-53(Fe).[34]

Findings of N₂ adsorption–desorption curves (BET) and Barrett–Joyner–Halenda (BJH) pore size distribution investigations are presented in Fig. 2c and Table 1. APT and hybrid materials are classified as class II adsorption isotherms according to the worldwide IUPAC (Fig. 2c), and MIL-53(Fe) is classified as a class IV isotherm.[35] Both APT and the hybrid material display hysteresis loops, showing the existence of mesoporous pronounced increase in N₂ adsorption at $P/P_0 >$ 0.95, and the adsorption–desorption isotherm displayed a marked alteration with a distinct hysteresis loop, indicating the existence of mesoporous and partially macroporous structures.[34] To demonstrate that the BET curves of APT@MIL53(Fe)-50 have decelerated, the reduction in hysteresis loops suggests the presence of a limited quantity of mesoporous and certain macroporous structures. Those discussions are substantiated in Table 1, demonstrating that the hybrid material enhances the specific surface area, pore volume, and pore diameter to varying extents with increased APT hybridizing. The findings indicate that the adsorption capacity of APT@MIL53(Fe)-70 surpasses that of APT@MIL53(Fe)-50.

The prepared materials were characterized by Fourier-transform infrared (FT-IR) spectroscopy for surface groups (Fig. 2d). A spectrum of absorption of APT in the 3618 cm⁻¹ band is ascribed to the stretching vibrations of Al^{3+} associated with hydroxyl and coordination water.[36] This 3554 cm⁻¹ absorption peak is ascribed to the hydroxyl vibrations in Mg–OH,[37] while the broad peaks within the range of 3500–3000 cm⁻¹ are attributed to the –OH group, the dual absorbent peaks at 988 cm⁻¹ and 1037 cm⁻¹ are ascribed to Si–O–Si bonding.[38,39] MIL-53(Fe) exhibits unsymmetrical stretching vibration peaks of the functional group on the organic ligand at 1390 cm⁻¹, 1556 cm⁻¹, and 1670 cm⁻¹, corresponding to C=O in the carboxyl functionality, C=C in the benzene ring, and O–C in the carboxyl the substituted aromatic compounds is observed at 744 cm⁻¹.[40] Post-hybridizing, the absorption spectra of APT@MIL53(Fe)-50 and APT@MIL53(Fe)-70 exhibited enhanced smoothness in Al–OH and Mg–OH.[41] Additionally, new characteristic peaks of MIL-53(Fe) emerged,[42,43] with a noticeable rightward shift in peak positions and increased peak absorption intensity. This suggests that APT interacted with MIL-53(Fe), confirming the successful synthesis of APT@MIL53(Fe)-50 and APT@MIL53(Fe)-70.

Scanning electron microscopy (SEM) was conducted on APT, MIL-53(Fe), and the synthesized APT@MIL53(Fe)-70 and APT@MIL53(Fe)-50 to examine their surface microstructures, with the results presented in Fig. 3a displays that APT exhibits a uniform fibrous rod-like morphology. At the specified magnification, the APT surface appears smooth. The rod length measures approximately 1 μm, corroborating prior findings.[27] At the same magnification, MIL-53(Fe) shows a biconical hexagonal prism structure and a hexagonal bipyramidal structure,[14,44] characterized by smooth and dense surfaces (Fig. 3c and d). APT hybridizing on MIL-53(Fe) crystals results in the material transitions from hexagonal bipyramid to biconical hexagonal prism morphology with increasing hybridizing amount.[14,45] This view clarifies that the physicochemical properties are enhanced post-hybridization, as evidenced by the prior PXRD patterns and BET analysis, with a rise in specific surface area and expanded pore size. The elemental distribution results from the EDS of the hybrid material are presented (Fig. 3i). It is obvious that the rod-shaped crystals are equally dispersed across the surface (ESI: Fig. S3†). One aspect is that Fe, Si, Al, O, N, Mg, and C are uniformly distributed on the surface of the hybrid material. All elevated concentrations of Fe and Si confirm the efficacy of the hybrid material, and the biconical hexagonal prismatic structure of the seven elements is distinctly observable in the EDS diagrams.[27,35,42] The characterization confirms that demonstration of APT distribution on MIL-53(Fe) surface and successful preparation of hybrid material.

4. Exploration of adsorption factors

4.1 Effect of contact time

Initially, the duration of contact between antibiotics in agricultural wastewater and hybrid material significantly influences the adsorption accumulation. By comparing the impact of an
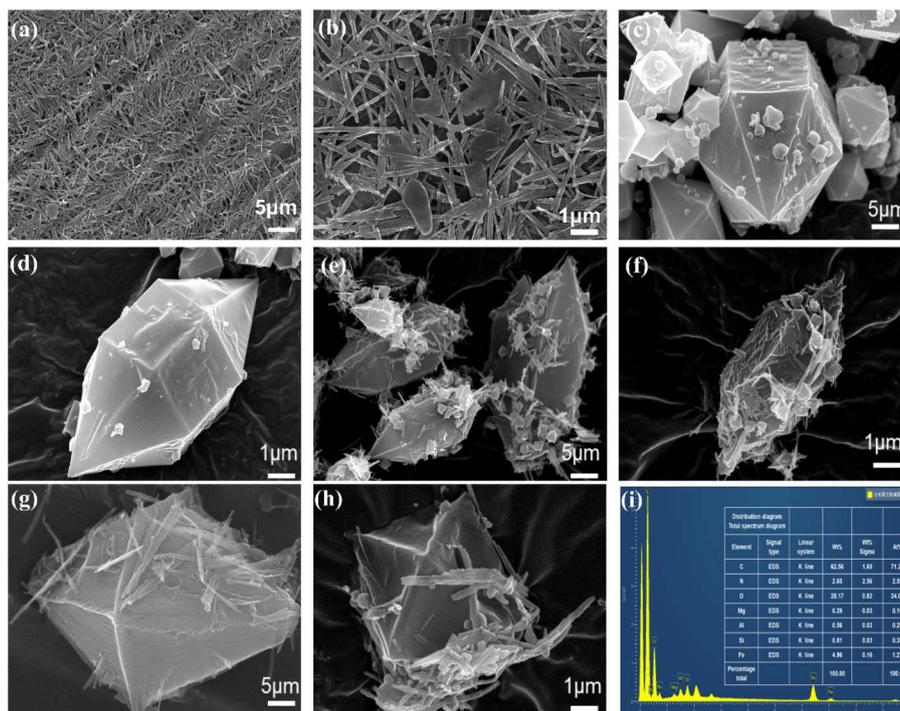
Fig. 3 SEM images of different samples (a and b) APT; (c and d) MIL-53(Fe); (e and f) APT@MIL53(Fe)-70; (g and h) APT@MIL53(Fe)-50; (i) EDS elemental image results for APT@MIL53(Fe)-70.

adsorbent concentration of 0.10 g L^{-1} of APT@MIL53(Fe)-70 on TC and APT@MIL53(Fe)-50 on OTC adsorption over 300 min (Fig. 4a and b), the graphs are refined to illustrate the in-solution UV absorption of the residual TC/OTC (ESI: Text 1†).

The adsorption process has three phases: the quick adsorption phase, the adsorption inflection phase, and the adsorption equilibrium phase, with the adsorption phases depicted in the simplified graph (Fig. 4a and b). A significant rise in TC/OTC
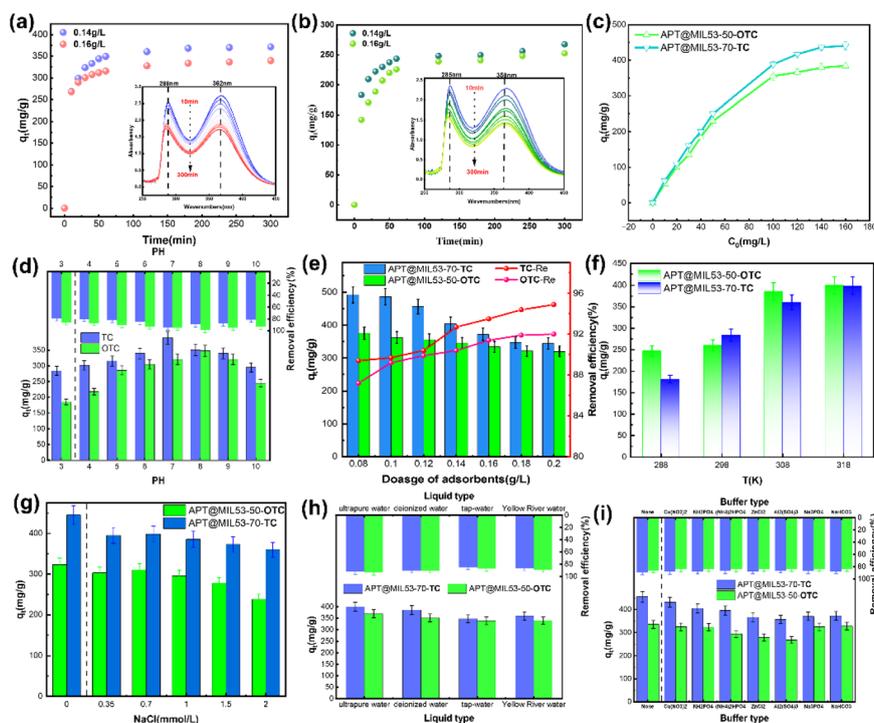

Fig. 4 Effect of time (a) TC (b) OTC; effect of initial concentration (c); effect of solution pH (d); effect of adsorbent additive (e); effect of ionic strength (f); effect of temperature (g); effect of actual water (h); effect of actual buffer system (i).

adsorption occurred during the initial 20 min, attributed to the elevated concentration of TC/OTC in the water at the onset of the reaction and the ample availability of active surface sites on the adsorbent, leading to adsorption driven by a substantial adsorption force.[46] Adsorption inflection points transpire between 20 to 60 min, during which the surface active sites are partially occupied, resulting in a deceleration of the adsorption process. Complete adsorption equilibrium is attained around 120 min, after which the adsorption quantity stabilizes. Adsorbent concentration increases active sites on the hybrid material surface but reduces effective collision, causing adsorption equilibrium first at 0.14 g L^{-1}, indicating superior adsorption per unit of removal.

4.2 Effect of initial concentration

Secondly, a spectrum of TC/OTC with an initial concentration of 10–160 mg L^{-1} was investigated (ESI: Text 1†), revealing differences in the adsorption capacities of APT@MIL53(Fe)-70 and APT@MIL53(Fe)-50, respectively (Fig. 4c). An increase in initial concentration leads to a larger gradient gap between the adsorbent surface and adsorption-driven force.[45] At an initial concentration of TC/OTC of 100 mg L^{-1}, the adsorption rate diminished following the inflection point of the adsorption quantity. Therefore, 100 mg L^{-1} was selected as the beginning concentration for the adsorbents TC and OTC.

4.3 Effect of pH

The influence of pH, ranging from 3.0 to 10.0, on the adsorption of TC/OTC was examined (ESI: Text 1†), as pH alters the surface charge of the hybrid material (Fig. 4d).[47] At pH = 3, TC mostly occurs as TCH$_3^+$ in the solution due to the high concentration of H$^+$, resulting in a positively charged surface of the hybrid material.[22] In this case, electrostatic repulsion leads to a lower adsorption performance of the adsorbent material for TC. TC removal efficiency gradually increased to 94.5% as the solution pH increased to 7 when TC in the form of TCH$_2^\pm$ and APT@MIL53(Fe)-70 produced electrostatic gravitational interactions to promote the adsorption performance of TC. When the solution is increased to 10, TC exists as TCH$^-$ and TC^{2-} sequentially, resulting in a rise of negative charge on the surface of the adsorbent material APT@MIL53(Fe)-70, hence boosting the adsorption process through the electrostatic hindrance effect. This discussion suggests that APT@MIL53(Fe)-70 preferentially adsorbs tetracycline at ideal adsorption pH = 7.[48] While the solution is acidic, the high concentration of H$^+$ disrupts the ionization equilibrium of OTC, leading to its predominant existence as H$_3$OTC$^+$. Concurrently, the surface of the APT@MIL53(Fe)-50 material acquires a positive charge due to protonation, which subsequently influences adsorption through electrostatic repulsion.[49]

As the solution approaches neutrality, the concentration of H$^+$ diminishes, resulting in the predominant presence of H$_2$OTC. The adsorbent surface of the material acquires a positive charge, while a minor fraction of the OTC exists in its negatively charged ionized form, facilitating electrostatic attraction and thereby enhancing the adsorption of OTC to

optimize performance. Ionization of OTC mainly occurred as HOTC when the solution pH was raised to 10. However, the surface of the hybrid material was positively charged due to 7.49 < pH < pH$_{pzc}$ = 8.49. OTC achieved the maximum adsorption removal rate of 98.7% at pH = 8, primarily due to electrostatic attraction. Continued elevation of the solution to 10 amplifies the negative charge on the surface, hence intensifying the electrostatic repulsion of HOTC$^-$ and OTC^{2-}, which obstructs OTC adsorption. Evidence indicates that the optimal adsorption pH = 8, and APT@MIL53(Fe)-50 exhibit selectivity for OTC adsorption.[48] Electrostatic interactions are impacted by acidic and alkaline environments, where pore filling dominates adsorption.

4.4 Effect of different adsorbent concentrations

Fourthly, the impact of heterogeneous material addition on adsorption performance was examined, revealing a substantial increase in adsorption capacity with greater amounts of heterogeneous material added (Fig. 4e). A maximum dosage of 405.1 mg g^{-1} (R_e 92.7%) was attained when APT@MIL53(Fe)-70 was delivered at a concentration of 0.14 g L^{-1}. The highest absorption dose at APT@MIL53(Fe)-50 was 334.0 mg g^{-1} (R_e 91.4%) at a concentration of 0.16 g L^{-1}. As the hybridized material is incrementally added, the adsorption active sites and pore space on the material's surface become adequate, resulting in a gradual enhancement of adsorption performance.

4.5 Effect of adsorption system temperature

Temperature changes in TC/OTC adsorption, with conversion rates over 90% (Fig. 4f). Hybrid materials exhibit efficiency, with APT@MIL53(Fe)-70 and APT@MIL53(Fe)-50 adsorbed at 308 K, aligning with the ideal temperature range for antibiotic adsorption (ESI: Table S2†).

4.6 Effect of ionic strength

When the ionic strength of NaCl in the adsorption system increases, the fluctuation of OTC is less than 50 mg g^{-1}, but the variation in the adsorption quantity of TC remains minimal, indicating that the adsorption performance of TC is more stable (Fig. 4g). Despite the minimal impact on adsorption at varying ionic strengths, selectivity for the adsorption of TC by APT@MIL53(Fe)-70 and OTC by APT@MIL53(Fe)-50 persists in the presence of various ions, corroborating the conclusions from the prior discussion.[48]

4.7 Effects on adsorption under simulated agricultural wastewater conditions

Crucially, farmers typically utilize tap or river water to minimize costs in actual agricultural aquaculture. This employed ultrapure water as a blank control, while deionized water, tap water, and Yellow River water served as comparative groups (Fig. 4h). The findings indicate that even in complex water bodies, the adsorption effect is negligible, suggesting that adsorbent materials perform selectively in real water environments and possibly applicability in actual water bodies.

The adsorption behavior of $Cu(NO_3)_2$, KH_2PO_4, $(NH_4)_2HPO_4$, $ZnCl_2$, $Al_2(SO_4)_3$, Na_3PO_4, and $NaHCO_3$ in actual agricultural wastewater was modeled, demonstrating its efficacy for the removal of TC/OTC in practical buffer systems (Fig. 4i). Even though the adsorption is stable in common agricultural waters and simulated agricultural wastewater carried out to illustrate the selectivity and practical application possibilities of APT@MIL53(Fe)-70 for TC adsorption and APT@MIL53(Fe)-50 for OTC adsorption.

5. Adsorption discussions

5.1 Adsorption kinetics analysis

Adsorption kinetics of TC/OTC over 5 hours were undertaken to evaluate the removal effectiveness of TC/OTC (Fig. 5a and b), and the adsorption data across temperature gradients were analyzed through model fitting utilizing pseudo-first-order and pseudo-second-order kinetics models. Fig. 5a and d show the adsorption of TC/OTC with time at four temperature gradients. The pseudo-second-order kinetic model in Fig. 5b and e fits the actual adsorption point better than the pseudo-first-order (ESI: Table S3†), indicating that the TC/OTC adsorption belongs to chemisorption. Temperature gradients corresponding to equilibrium adsorption at 288 K, 298 K, 308 K, and 318 K are ascribed to the increased energy available at elevated temperatures, which enhances the adsorption characteristics of the materials.

5.2 Adsorption isotherm analysis

The adsorption isotherm is the primary model elucidating the transfer of TC/OTC from liquid to solid phases in the environment.[47] The Langmuir and Freundlich isotherm models were employed to analyze the adsorption data and elucidate potential adsorption mechanisms through the fitted correlation data and fundamental thermodynamic principles.[50] In this context, K_L (L mg^{-1}) represents the Langmuir isotherm constant, K_F (L g^{-1}) denotes the Freundlich isotherm constant, and $1/n$ indicates the surface heterogeneity of the adsorbed material.[11] APT@MIL53(Fe)-70 has absorbed TC, as shown in Fig. 5c. The quantity of adsorption increased with the rise in starting concentration, attributed to the significant adsorption driving force between the high concentration of TC and the adsorbent material.[51] As the system temperature rose, the TC equilibrium adsorption increased, indicating that the adsorption process may be thermally driven.[52] The fitting results indicated that the correlation coefficients derived from monolayer of Langmuir adsorption model were all $R^2 > 0.99$. This calculated equilibrium adsorption at 308 K was 600.4 mg g^{-1}, achieving a removal efficiency of 93.5%. It further substantiated that the adsorption of TC was monolayer and involved chemical adsorption.[50] Fig. 5f clarifies the isothermal linearity fitting of OTC adsorption by APT@MIL53(Fe)-50 under a temperature gradient. The fitting results indicating that the correlation coefficient R^2 of the Langmuir adsorption model fitting is superior to that of the Freundlich adsorption model (ESI: Table S4†). This suggests that the adsorption of OTC is a monolayer adsorption process. The equilibrium adsorption capacity of OTC at 308 K was calculated to be 537.7 mg g^{-1}, achieving a removal efficiency of 91.4%. This Langmuir fitting of TC/OTC adsorption across a temperature gradient of 288–318 K, with $0 < K_L < 1$, reflects a homogeneous adsorption process.[53] Furthermore, the $1/n$ value in the Freundlich fitting data aligns with the concentration's influence on adsorption quantity within the range of 0–1.[17] Adsorption becomes challenging when $1/n$ exceeds 2; however, the $1/n$ values in the provided table are significantly below 2, indicating that adsorption is readily achievable.[17,54] Better selectivity and higher adsorption capacity than existing materials.[17,22,54]

5.3 Thermodynamic analysis of adsorption

The thermodynamic energy change of the adsorption process was examined by Gibbs free energy (ΔG), enthalpy change (ΔH),
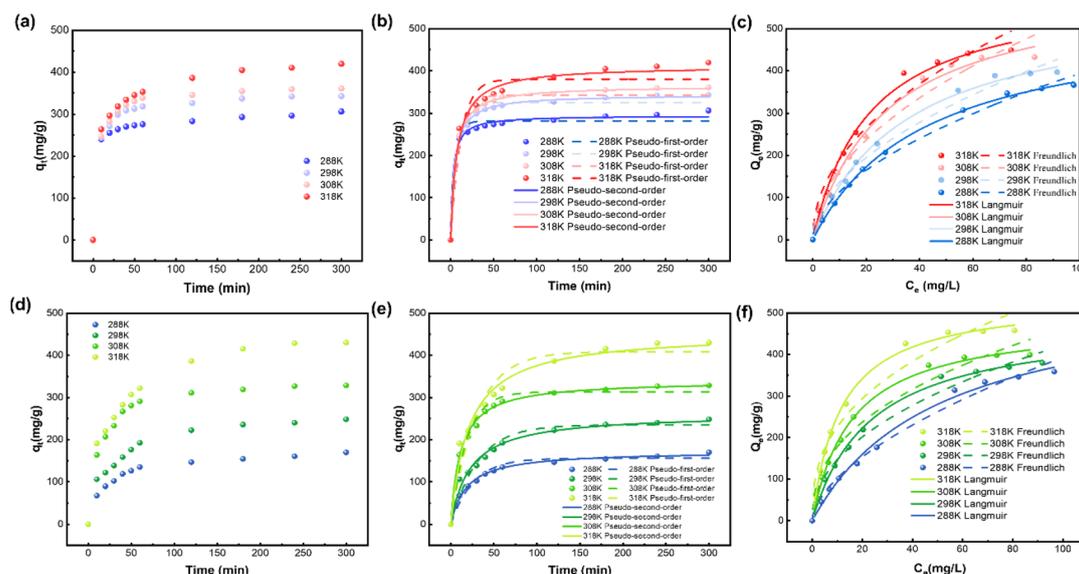

Fig. 5 Kinetic study of TC (a and b), OTC (d and e); isotherm fitting of TC (c), OTC (f).

and entropy change (ΔS) (ESI: Fig. S4 and Table S5†).[55] All ΔG values (-4.06 kJ mol^{-1} to -6.48 kJ mol^{-1}) during TC adsorption were negative, and the absolute value of ΔG increased with rising system temperature, indicating that the adsorption of TC by APT@MIL53(Fe)-70 was spontaneous. Furthermore, the elevation of temperature enhanced the spontaneity of the adsorption process. $\Delta H > 0$ during adsorption signifies that the adsorption process of TC is endothermic, and an increase in temperature enhances adsorption, aligning with prior findings.[56] $\Delta S > 0$ during adsorption signifies that the adsorbent exhibits an affinity for TC and elucidates the enhancement of solid–liquid interfacial disorder on the material's surface post-adsorption, consistent with the principles of chemical adsorption.[57] In the case of the adsorption of APT@MIL53(Fe)-50 on OTC, the Gibbs free energy $\Delta G < 0$, enthalpy change $\Delta H > 0$, and entropy change $\Delta S > 0$ signify that the adsorption process is a spontaneous endothermic reaction, favored by an increase in temperature and a rise in disorder.

6. Adsorption mechanism analysis

A comparison of FT-IR spectra of the hybrid material before and after the adsorption of TC/OTC reveals that the absorption peaks of Al–OH, Mg–OH, and –OH present a smoother profile following the adsorption of TC by APT@MIL53(Fe)-70, indicating the involvement of –OH in the adsorption process of TC (Fig. S7† and 6a). The weak absorption of C=O in the organic ligand region indicates that the –COOH groups on the APT surface of the APT@MIL53-70(Fe) material may be hydrogen-bonded to NH$_2$ and a significant quantity of –OH from TC. The widening of the C=C stretching vibrational peaks in the aromatic rings is ascribed to the π–π stacking interaction between the aromatic rings of the adsorbent material and those in the adsorbate TC.

Their AlOH, MgOH, and –OH groups in the APT@MIL53(Fe)-50 material structure are all equally engaged in OTC adsorption (Fig. S7† and 6b). Furthermore, the –COOH groups on the material surface may engage in hydrogen bonding with the NH$_2$ and numerous –OH groups of the OTC, leading to its adsorption. Consequently, the C=C stretching vibrational peaks on the aromatic ring broaden, and the C–H absorption intensifies, attributed to π–π stacking between the aromatic ring of the adsorbent material and that of the OTC. After adsorption, the distinctive Si–O–Si absorption peaks of the hybrid material remained evident, signifying that the adsorption of TC/OTC did not compromise the integrity of the adsorbed material, allowing for its recyclability.

Comparison of the XRD plots before and after the adsorption of TC/OTC (Fig. S8†, 6c and d) reveals alterations in the crystal structure of the hybrid surface of the material, thereby confirming the adsorption of TC/OTC by the hybrid material. After APT@MIL-53-70 adsorption of TC, the crystal plane of 101 shifted to 12.5°, possibly due to chemical adsorption. Following OTC adsorption with APT@MIL-53-50, the 101 crystal plane changed to 12.58° and the peak increased, which might be attributed to the synergistic effect of surface and chemical interaction.

The XPS examination of APT, hybrid material, and MIL-53(Fe) indicates that APT has typical elements such as Mg, Si, and Al, whereas MIL-53(Fe) comprises elements including Fe, N, O, and C. Comprehensive spectrum analyses of APT@MIL53(Fe)-70 and APT@MIL53(Fe)-50 reveal the presence of Fe and N, signifying effective hybridization and synthesis. All spectra in this investigation were adjusted and calibrated using the C 1s reference at 284.8 eV to analyze the material before and following adsorption. APT@MIL53(Fe)-70 (Fig. 6f) 284.8 eV, 288.50 eV, and 288.62 eV correspond to C=C, C–N from benzoic acid, and O–C=O from the carboxylic acid moiety, respectively.[30] The enhancement in the invariant strength of C=C binding energy following adsorption is attributed to the hexagonal carbon atoms present in the adsorbed tetracycline. The bond energies of C–N and O–C=O are reduced by 0.12 eV and 0.15 eV, respectively, indicating their participation in the adsorption process of tetracycline,[58] which aligns with the FT-IR analyses. In Fig. 6g, the N 1s analytical spectra at 402.23 eV and 400.61 eV correspond to N$^+$ and N–C, respectively, exhibiting shifts of 0.90 eV and 0.51 eV towards lower binding energy following the adsorption of TC. This O 1s analysis result indicates that the binding energies at 531.62 eV, 532.50 eV, and 532.45 eV correspond to C=O, –OH, and C–O, respectively. Following adsorption, all three binding energies shift towards higher values, with a notable increase in the intensity of the –OH signal, likely due to the presence of numerous hydroxyl groups in the TCs post-adsorption.[59] This Fig. 6f illustrates the C 1s analysis of APT@MIL53(Fe)-50 before and following the adsorption of OTC. The binding energies before adsorption are 284.80 eV, 286.43 eV, and 288.59 eV, corresponding to the C=C, C–N, and O–C=O bonds, respectively. Post-adsorption, the C–N bond exhibits a shift of 0.22 eV towards lower binding energy, while the O–C=O bond shifts by 0.07 eV towards higher binding energy, indicating the involvement of C–N and O–C=O in the OTC adsorption process. These double-shouldered peaks following N 1s adsorption (Fig. 6g) exhibited a shift of 0.86 eV for N$^+$ and 0.48 eV for C–N bonds towards lower binding energies, accompanied by a reduction in peak intensities post-adsorption. In the O 1s spectrum (Fig. 6h), the peaks at 531.62 eV, 532.45 eV, and 532.50 eV correspond to C=O, –OH, and C–O (Fig. 6k), respectively. Following adsorption, C=O and –OH shifted 0.16 eV and 0.28 eV towards lower binding energy.

The increase in –OH intensity, attributed to the substantial number of hydroxyl groups adsorbed on the OTC surface, caused the C–O peak to shift 0.32 eV towards higher binding energy. This indicates that C=O and C–O participate in the adsorption of OTC by APT@MIL53(Fe)-50, corroborating the FT-IR analysis results.

Additionally, both TC and OTC comprise stable linear tetracyclic nuclei with fused four rings and benzene ring structures, featuring various ionizable functional groups.[22] In contrast, the APT@MIL53(Fe)-70 and APT@MIL53(Fe)-50 structures exhibit numerous exposed hexagonal carbon atom arrangements, which are prone to π–π stacking interactions.[36,60] Functional groups in the TC/OTC structure, including hydroxyl, phenolic, and dimethyl amino groups establish hydrogen bonds with –OH on the APT@MIL53(Fe)-70 and
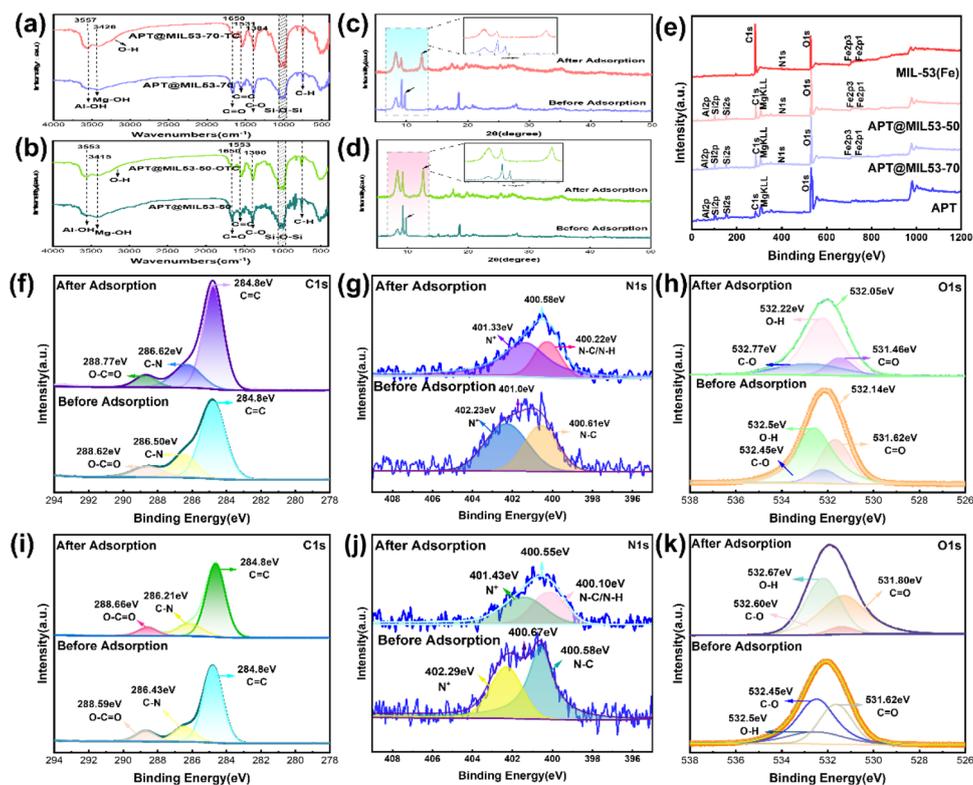
Fig. 6 (a, c, f, g and h) FT–IR spectra, XRD spectra, C 1s, N 1s, O 1s, before and after adsorption of TC, (b, d, i, j and h) FT–IR spectra, XRD spectra, C 1s, N 1s, O 1s, before and after adsorption of OTC, (e) full scan spectra of APT, MIL–53(Fe), APT@MIL53-70(Fe), APT@MIL53-50(Fe).

APT@MIL53(Fe)-50 surfaces,[7] corroborating the FT-IR data.[61] After TC adsorption with APT@MIL53-70, the specific surface area was reduced by 1.66 times, while the pore size was reduced by 5.31 nm. During OTC adsorption, the specific surface area of APT@MIL53-50 was dramatically reduced, as was the pore size, by 8.32 nm (Table 1). The BET test results indicated a significant reduction in specific surface area, pore volume, and pore diameter before and after adsorption in APT@MIL53(Fe)-70 with TC and APT@MIL53(Fe)-50 with OTC, suggesting pore filling during adsorption. The ideal pH for effective adsorption is pH = 7, with a pH_{pzc} of 7.54 (Fig. S9†). At this pH, the positively charged APT@MIL53(Fe)-70 surface engages in electrostatic interactions with TCH^{2-} in solution, resulting in the most substantial mutual attraction, and the adsorption mechanism is governed by electrostatic attraction effects.[7,59] OTC achieves the maximum adsorption removal rate and the largest adsorption capacity at pH = 8 (Fig. S9†), where pH = 8 < pH_{pzc} = 8.49. At this pH, OTC predominantly occurs as $HOTC^-$, facilitating its removal through electrostatic attraction.[23,62]

7. Recycling property

The recyclability of adsorbent materials is frequently associated with their economic advantages and serves as a crucial indicator of their practical application potential.[56] The results of the adsorption cycle regeneration of APT@MIL53(Fe)-70 and APT@MIL53(Fe)-50 are shown in Fig. 7, APT@MIL53(Fe)-70 retains a high adsorption capacity after six recycling cycles,

subsequently exhibiting a consistent adsorption capacity, indicating stable performance for TC. Furthermore, after three cycles of OTC adsorption, the adsorption capacity of APT@MIL53(Fe)-50 remains stable, demonstrating greater stability than the former. Furthermore, APT@MIL53(Fe)-50 exhibited a consistent adsorption capacity for OTC after three cycles of adsorption, demonstrating its persistent adsorption efficacy for TC.
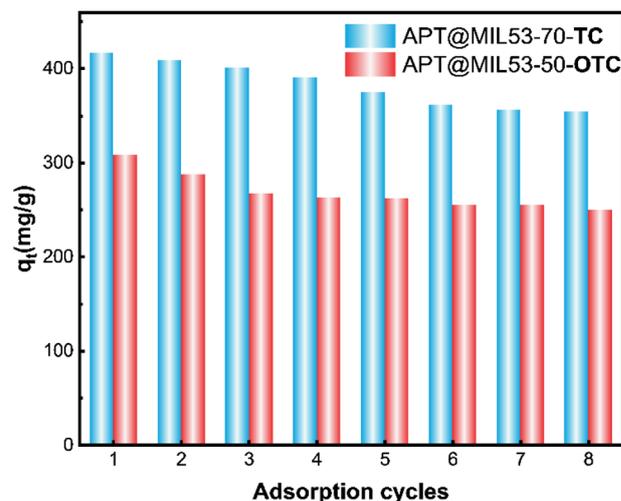

Fig. 7 Adsorption performance of recycling cycle.

8. Conclusions

In conclusion, this study is the initial effort to investigate the selective adsorption of TC/OTC with varying APT hybridizing levels to achieve efficient removal of typical TC/OTC from agricultural wastewater. The adsorption selectivity of hybrid material for TC/OTC was confirmed that APT@MIL53(Fe)-70 and APT@MIL53(Fe)-50 exhibited selectivity for the adsorption of TC and OTC, respectively. APT@MIL53-X showed significant chemical stability in the 3–10 pH range. Furthermore, the kinetic, isothermal and adsorption thermodynamic studies of the adsorption data at gradient temperatures showed that the pseudo-second-order kinetic and Langmuir models were more relevant to the adsorption process, which verified that the adsorption of TC/OTC was a chemisorption and monolayer adsorption process. Besides equilibrium adsorption capacity of TC was calculated to be 600.4 mg g^{-1} (removal efficiency of 94.5%) and that of OTC was 537.7 mg g^{-1} (removal efficiency of 98.7%) at 308 K, based on the Langmuir adsorption model. Several physicochemical features of materials before and after adsorption indicate that TC/OTC adsorption involves electrostatic interactions, π–π stacking, hydrogen bonding, and pore filling. APT@MIL53-X showed stable desorption, APT@MIL53(Fe)-70 and recycling performance, maintaining a stable adsorption amount and chemical stability after six adsorption–desorption cycles of use, which proved that APT@MIL53-X has application possibilities for the agricultural wastewater treatment process. Overall, the present work provides a novel and environmentally sustainable approach for the removal of TC/OTC from agricultural wastewater in substantial volumes.

Data availability

All data generated or analysed during this study are included in this published article and its ESI† files.

Author contributions

Jiaolan Liu, Xiaoyan Wang, Yuzhu Yang designed the samples and performed the experiments; Jiaolan Liu wrote the paper with support from Wei Sheng Liu and Wei Liu. All authors contributed to the general discussion.

Conflicts of interest

The authors declare that they have no conflict of interest.

Acknowledgements

Notes and references

1 A. Waheed, N. Baig, N. Ullah and W. Falath, *J. Environ. Manage.*, 2021, **287**, 112360.
2 R. Daghrir and P. Drogui, *Environ. Chem. Lett.*, 2013, **11**, 209–227.
3 J. Hou, C. Wang, D. Mao and Y. Luo, *Environ. Sci. Pollut. Res.*, 2015, **23**, 1722–1731.
4 F. Baquero, T. M. Coque, J.-L. Martínez, S. Aracil-Gisbert and V. F. Lanza, *Front. Microbiol.*, 2019, **10**, 2892–2906.
5 T. Kivits, H. P. Broers, H. Beeltje, M. van Vliet and J. Griffioen, *Environ. Pollut.*, 2018, **241**, 988–998.
6 S. Suzuki, S. Nakanishi, M. Tamminen, T. Yokokawa, Y. Sato-Takabe, K. Ohta, H.-Y. Chou, W. I. Muziasari and M. Virta, *Sci. Total Environ.*, 2019, **669**, 649–656.
7 J. Tang, L. Zong, B. Mu, Y. Kang and A. Wang, *Korean J. Chem. Eng.*, 2018, **35**, 1650–1661.
8 Y. Bai, X. Ruan, X. Xie and Z. Yan, *Environ. Pollut.*, 2019, **248**, 438–447.
9 L. Zhou, Q. Jiang, S. Sun, Y. Wu, T. Li, Y. Gao, W. Zhang, L. Tian, M. Tang and X. Wang, *Sep. Purif. Technol.*, 2022, **286**, 120481.
10 R. Yue and X. Sun, *Sep. Purif. Technol.*, 2021, **279**, 119796–119807.
11 P. Su, Q. Huo, C. Zhang, Z. Wang and Y. Qiao, *J. Clean. Prod.*, 2024, **461**, 142395.
12 B. K. Bhangi and S. Ray, *Polym. Eng. Sci.*, 2022, **63**, 249–266.
13 R. Pulicharla, S. K. Brar, T. Rouissi, S. Auger, P. Drogui, M. Verma and R. Y. Surampalli, *Ultrason. Sonochem.*, 2017, **34**, 332–342.
14 J. Yu, J. Cao, Z. Yang, W. Xiong, Z. Xu, P. Song, M. Jia, S. Sun, Y. Zhang and J. Zhu, *J. Colloid Interface Sci.*, 2020, **580**, 470–479.
15 M. Ahmadi, H. R. Motlagh, N. Jaafarzadeh, A. Mostoufi, R. Saeedi, G. Barzegar and S. Jorfi, *J. Environ. Manage.*, 2017, **186**, 55–63.
16 S. M. Ghoreishian, G. S. R. Raju, E. Pavitra, C. H. Kwak, Y.-K. Han and Y. S. Huh, *Appl. Surf. Sci.*, 2019, **489**, 110–122.
17 Q. Song, Y. Fang, Z. Liu, L. Li, Y. Wang, J. Liang, Y. Huang, J. Lin, L. Hu, J. Zhang and C. Tang, *Chem. Eng. J.*, 2017, **325**, 71–79.
18 A. Abbasnia, A. Zarei, M. Yeganeh, H. R. Sobhi, M. Gholami and A. Esrafili, *Inorg. Chem. Commun.*, 2022, **145**, 109959.
19 Q. Wang, Q. Gao, A. M. Al-Enizi, A. Nafady and S. Ma, *Inorg. Chem. Front.*, 2020, **7**, 300–339.
20 Z. Zhang, Y. Chen, Z. Wang, C. Hu, D. Ma, W. Chen and T. Ao, *Appl. Surf. Sci.*, 2021, **542**, 148662.
21 P. L. Llewellyn, P. Horcajada, G. Maurin, T. Devic, N. Rosenbach, S. Bourrelly, C. Serre, D. Vincent, S. Loera-Serna, Y. Filinchuk and G. Férey, *J. Am. Chem. Soc.*, 2009, **131**, 13002–13008.
22 P.-H. Chang, Z. Li, T.-L. Yu, S. Munkhbayer, T.-H. Kuo, Y.-C. Hung, J.-S. Jean and K.-H. Lin, *J. Hazard. Mater.*, 2009, **165**, 148–155.
23 S. Jiao, S. Zheng, D. Yin, L. Wang and L. Chen, *J. Environ. Sci.*, 2008, **20**, 806–813.
24 Y. Xie, D. Shao, X. Lu, T. Hayat, N. S. Alharbi, C. Chen, G. Song, D. Chen and Y. Sun, *Ind. Eng. Chem. Res.*, 2018, **57**, 7533–7543.
25 D. Mukherjee, P. Das, G. N. Prasad, A. R. Katha, S. Gumma and B. Mandal, *Sep. Purif. Technol.*, 2022, **294**, 121217.

26 W. Xiong, G. Zeng, Z. Yang, Y. Zhou, C. Zhang, M. Cheng, Y. Liu, L. Hu, J. Wan, C. Zhou, R. Xu and X. Li, *Sci. Total Environ.*, 2018, **627**, 235–244.

27 G. Wang, R. Guo, W. Wang and W. Liu, *J. CO2 Util.*, 2020, **42**, 101303.

28 X. Fang, S. Wu, Y. Wu, W. Yang, Y. Li, J. He, P. Hong, M. Nie, C. Xie, Z. Wu, K. Zhang, L. Kong and J. Liu, *Appl. Surf. Sci.*, 2020, **518**, 146226.

29 T.-H. Wang, T.-Y. Liu, D.-C. Wu, M.-H. Li, J.-R. Chen and S.-P. Teng, *J. Hazard. Mater.*, 2010, **173**, 335–342.

30 Z. Zhu, W. Fan, Z. Liu, H. Dong, Y. Yan and P. Huo, *J. Photochem. Photobiol., A*, 2018, **359**, 102–110.

31 X. Zheng, S. Qi, Y. Cao, L. Shen, C. Au and L. Jiang, *Chin. J. Catal.*, 2021, **42**, 279–287.

32 D. Yuan, C. Shang, J. Cui, W. Zhang and Y. Kou, *Environ. Res.*, 2023, **216**, 114616.

33 X. Wang, W. Zhang, X. Zhang, L. Ran, Q. Zhao, B. Zou, L. Zhou and Z. Ye, *J. Clean. Prod.*, 2022, **348**, 131385.

34 L. Lu, X.-Y. Li, X.-Q. Liu, Z.-M. Wang and L.-B. Sun, *J. Mater. Chem. A*, 2015, **3**, 6998–7005.

35 Z. Zhang, X. Chen, Y. Tan, C. Jiang, H. Wang and S. Zhang, *Chem. Eng. J.*, 2022, **441**, 135881.

36 Y. Liu, Y. Liu, H. Wang, L. Dong and D. Di, *J. Chem. Technol. Biotechnol.*, 2018, **93**, 2331–2340.

37 X. Liu, X. Xu, J. Sun, A. Alsaedi, T. Hayat, J. Li and X. Wang, *Chem. Eng. J.*, 2018, **343**, 217–224.

38 K. Li, Y. Zhang, X. Zhang, B.-J. Ni, Y. Wei, B. Xu and D. Hao, *CrystEngComm*, 2022, **24**, 3064–3073.

39 S. Masoumi, F. F. Tabrizi and A. R. Sardarian, *J. Environ. Chem. Eng.*, 2020, **8**, 103601–103610.

40 Z. Sun, X. Wu, K. Qu, Z. Huang, S. Liu, M. Dong and Z. Guo, *Chemosphere*, 2020, **259**, 127389–127401.

41 C. Sophia A and E. C. Lima, *Ecotoxicol. Environ. Saf.*, 2018, **150**, 1–17.

42 S. Naeimi and H. Faghihian, *Environ. Toxicol. Pharmacol.*, 2017, **53**, 121–132.

43 C. C. Obi, M. N. Abonyi, P. E. Ohale, C. E. Onu, J. T. Nwabanne, C. A. Igwegbe, T. T. Kamuche and I. H. Ozofor, *Chem. Eng. J.*, 2024, **497**, 154767–154792.

44 N. Yuan, X. Zhang, T. Chen, H. Xu and Q. Wang, *J. Colloid Interface Sci.*, 2023, **646**, 438–451.

45 Y.-y. Zhang, Q. Liu, C. Yang, S.-c. Wu and J.-h. Cheng, *Environ. Pollut.*, 2019, **255**, 113226–113236.

46 L. Jiang, Y. Liu, S. Liu, X. Hu, G. Zeng, X. Hu, S. Liu, S. Liu, B. Huang and M. Li, *Chem. Eng. J.*, 2017, **308**, 597–605.

47 J. Dai, X. Meng, Y. Zhang and Y. Huang, *Bioresour. Technol.*, 2020, **311**, 123455–123463.

48 S. Kumari, A. Chowdhury, A. A. Khan and S. Hussain, *J. Hazard. Mater.*, 2021, **415**, 125750–125766.

49 G. Limousin, J. P. Gaudet, L. Charlet, S. Szenknect, V. Barthès and M. Krimissa, *Appl. Geochem.*, 2007, **22**, 249–275.

50 Q. Yu, R. Zhang, S. Deng, J. Huang and G. Yu, *Water Res.*, 2009, **43**, 1150–1158.

51 G. K. Ramesha, A. V. Kumara, H. B. Muralidhara and S. Sampath, *J. Colloid Interface Sci.*, 2011, **361**, 270–277.

52 J. Jin, Z. Yang, W. Xiong, Y. Zhou, R. Xu, Y. Zhang, J. Cao, X. Li and C. Zhou, *Sci. Total Environ.*, 2019, **650**, 408–418.

53 B. Wang, X. Xu, H. Tang, Y. Mao, H. Chen and F. Ji, *Appl. Surf. Sci.*, 2020, **528**, 147048–147058.

54 N. Li, L. Zhou, X. Jin, G. Owens and Z. Chen, *J. Hazard. Mater.*, 2019, **366**, 563–572.

55 J. Yan, X. Zuo, S. Yang, R. Chen, T. Cai and D. Ding, *J. Hazard. Mater.*, 2022, **424**, 48285–48295.

56 S. Xiaosan, S. Boyang, W. Yiru, Z. Jie, W. Sanfan and W. Nan, *RSC Adv.*, 2022, **12**, 19917–19928.

57 S. Senthilkumaar, P. Kalaamani and C. Subburaam, *J. Hazard. Mater.*, 2006, **136**, 800–808.

58 L.-l. Yu, W. Cao, S.-c. Wu, C. Yang and J.-h. Cheng, *Ecotoxicol. Environ. Saf.*, 2018, **164**, 289–296.

59 G. Zhang, S. Li, Y. Li and X. Dong, *Appl. Clay Sci.*, 2023, **246**, 107162–107169.

60 Y. Lin, S. Xu and J. Li, *Chem. Eng. J.*, 2013, **225**, 679–685.

61 A. M. Ealias and M. P. Saravanakumar, *J. Environ. Manage.*, 2018, **206**, 215–227.

62 X. Wang, Y. Wang, C. Zhao, Y. Zhu, Z. Sun, H.-J. S. Fan, X. Hu and H. Zheng, *Water Res.*, 2021, **202**, 117393–117406.